

DinoLizer: Learning from the Best for Generative Inpainting Localization

Minh Thong DOI^{1,2} Jan BUTORA² Vincent ITIER^{1,2} Jérémie BOULANGER²
Patrick BAS²

¹IMT Nord Europe, Institut Mines-Télécom, Centre for Digital Systems, F-59000 Lille, France

²Centre de Recherche en Informatique, Signal et Automatique de Lille, Avenue Henri Poincaré, 59655 Villeneuve d'Ascq, France

November 27, 2025

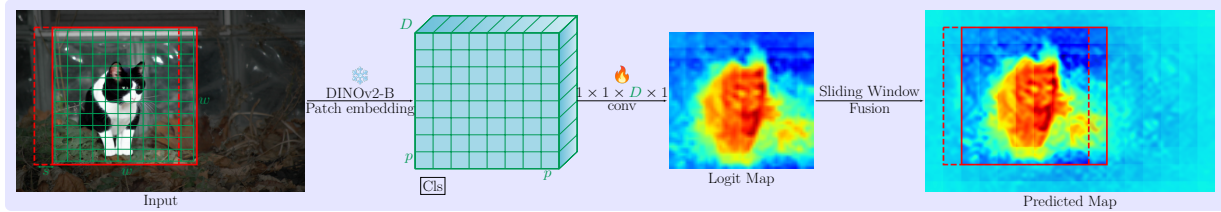


Figure 1: Principle of DinoLizer: the image is decomposed into a set of 504×504 overlapping crops which are fed to the DINOv2 model to provide embeddings of dimension d for each patch plus a class token which is not considered here. A 1×1 trainable convolutional layer is used to infer a logit map, which is then fused with other overlapping maps in order to provide, after thresholding, a localization mask.

Abstract

We introduce DinoLizer, a DINOv2-based model for localizing manipulated regions in generative inpainting. Our method builds on a DINOv2 model pretrained to detect synthetic images on the B-Free dataset. We add a linear classification head on top of the Vision Transformer’s patch embeddings to predict manipulations at a 14×14 patch resolution. The head is trained to focus on semantically altered regions, treating non-semantic edits as part of the original content. Because the ViT accepts only fixed-size inputs, we use a sliding-window strategy to aggregate predictions over larger images; the resulting heatmaps are post-processed to refine the estimated binary manipulation masks. Empirical results show that DinoLizer surpasses state-of-the-art local manipulation detectors on a range of inpainting datasets derived from different generative models. It remains robust to common post-processing operations such as resizing, noise addition, and JPEG (double) compression. On average, DinoLizer achieves a 12% higher Intersection-over-Union (IoU) than the next best model, with even greater gains after post-processing. Our experiments with off-the-shelf DINOv2 demonstrate the strong representational power of Vision Transformers for this task. Finally, extensive ablation studies compar-

ing DINOv2 and its successor, DINOv3, in deepfake localization confirm DinoLizer’s superiority. The code will be publicly available upon acceptance of the paper.

1 Introduction

Currently, Generative Artificial Intelligence (Gen-AI) poses serious threats to democracy since it can be used to create or amplify disinformation. When applied to digital images, the realism of the generated content increases after each new generation of models, and with the last generative methods, human observers are finding it increasingly difficult to distinguish between generated and authentic images. Generative inpainting is a byproduct of Gen-AI, which enables to locally remove or add subjects in the image. Using the last generation of image editing software, it is extremely easy to perform generative inpainting, and the detection of such manipulations is challenging because they blend authentic image parts with generated background (for object removal) or with a generated object (for object insertion). This difference explains why there are more forensic methods in the literature designed to detect generated images than to localize generative inpainting. However, if several detection meth-

Dataset	Real Source	Inpainting Schemes	Orig Bg	Fake Images
BtB [1]	Flickr30k	Fooocus [40], SDXL	✓	7.4k
B-Free [13]	MS-COCO [21]	SD2 Inpainting	✓, ×	10k
COCOG [12]	MS-COCO	GLIDE [27]	✓	512
TGIF [24]	MS-COCO	SD2, SDXL, Firefly	✓	4.1k
SAGI- SP [11] FR [11]	MS-COCO RAISE [7] OpenImages [17]	BrushNet, PowerPaint, HD-Painter, ControlNet Inpaint-Anything	✓ ×	2k 1.3k

Table 1: Overview of evaluation datasets with their real image sources, inpainting generators (SD = Stable Diffusion, BtB: Beyond the Brush, COCOG: CocoGlide). The presence of an original background (Orig Bg) or a background that is auto-encoded: × in the forged images is also indicated.

ods [13, 24] are also designed to detect inpainted images, the goal of localizing the manipulated region can be seen as an additional step towards explainability, and it can be very helpful to security agencies in their forensic tasks.

Many existing inpainting methods are based either on diffusion models such as Stable-Diffusion [31], Glide [26], or the commercial model from Adobe Firefly, but also other methods such as Fourier convolution-based methods and residual networks like LaMa [35] for object removal. On diffusion models, the inpainting methods such as Brushnet [15], PowerPaint [42], or Hd-painter [23] come from models that are fine-tuned, or adapted using extra input channels. They are used either to infer a masked part of the image during the backward diffusion process (for object insertion) or to replace an object with another. In order to obtain a better inpainting quality, the alignment between masked regions and semantic objects can be enforced by using Blip embeddings [38]. InpaintAnything [41] also proposes to mix the inpainting process with segmentation tools to perform high-quality inpainting.

Detection of generated images is possible by exploiting different biases occurring during the generation process. A semantic bias can originate from either using a small prompt or a model fine-tuned for a given class of images. Semantic features such as CLIP [30] are used to detect such a bias [28, 6], and are very efficient for this task. Another bias is linked to the generative process itself, it is then specific to the artifacts coming from GANs or LDM, such as color discrepancies [36] or specific correlations between neighboring pixels [22]. A third bias comes from the decoding step from the latent space to the pixel space, usually done using a Variational Auto-Encoder (VAE). It creates interpolation artifacts popular in the forensic community [16] which can be detected by Fourier analysis [37, 20, 10]. Recently, B-Free [13] pro-

posed a training strategy tailored to capture both the inherent bias of the generator and of the fingerprint of the VAE by removing the semantic bias thanks to inpainting techniques.

Image forgery localization (IFL) methods have received increased attention due to rapidly evolving sophisticated algorithms for local image tampering. TruFor [12] used a Transformer-based fusion of high-level image information and a noise signature extracted by the Noiseprint++ feature extractor to predict local discrepancies. SAFIRE [19] segments an image into regions having the same properties, and localizes manipulations as outlier regions. ManTra-Net [39] uses a fully convolutional network without any subsampling to predict local anomalies, and CAT-Net v2 [18] is another CNN that focuses on distortion in JPEG compression artifacts due to forgeries. In [34], the authors aim to find non-semantic features useful for IFL, and modify SparseViT [4] to extract context-irrelevant features by splitting the image into lattices of non-neighboring patches. However, most current methods have only been evaluated on traditional forgeries, such as copy-move and splicing, and not many works deal with AI-based inpainting with, e.g., diffusion models.

This paper presents a methodology for training DinoLizer, a localizer based on Vision Transformers (ViT) with several key characteristics:

- **Computational efficiency:** The training process requires minimal computational resources as it builds upon a frozen pre-trained DINOv2 model (already fine-tuned for image detection [13]), with only the linear classification head being trained for localization using the patch embeddings (patch tokens).
- **Inherited advantages:** The methodology benefits from the training strategy proposed in B-Free [13], which avoids semantic bias, an important property for Inpainting Forgery Localization (IFL) since manipulated images are semantically similar to real images.
- **Distinct approach:** Unlike B-Free, our approach treats auto-encoded regions as pristine, enhancing localization performance. This aligns with practical considerations: an auto-encoded image is not semantically manipulated since there is neither object removal nor object addition.
- **Extensibility:** We demonstrate that this methodology generalizes to newer ViT architectures, such as DINOv3.
- **Robust performance:** When combined with appropriate training using Dice Loss, data augmentation, and post-processing of localization masks, DinoLizer achieves excellent results across diverse ref-

erence databases, particularly when test images undergo post-processing such as noise addition, resizing, JPEG compression, or double-JPEG compression.

2 Related Works

Localization Methods Using Transformers Because Vision Transformers compute self-attention maps, they allow for encoding long-range dependencies and are ideal tools for object segmentation. As proposed by Segmenter [33], one popular approach is to adopt an encoder-decoder approach where the transformer plays the role of the encoder, and a linear mapping between the predicted mask and the different patch embeddings, followed by up-sampling, plays the role of the decoder. The same methodology was also adopted by the DINOv2 ViT [29] for image segmentation.

Regarding Image Forgery Localization, and to the best of our knowledge, SparseViT [34] is the only reference that proposes to use transformers for localization. To obtain a localization mask not focused only on the semantic content (several traces of the generation process, such as the VAE, are independent of the image semantics), the authors enforce sparse self-attention maps by training on disjoint subsampled subsets of patches.

Semantic and VAE bias removal Recently, different contributions have shown both excellent in-distribution and out-of-distribution detection (*i.e.* testing on unseen generators) performance by adopting training strategies designed to remove the semantic and/or VAE biases. The semantic bias usually comes from the fact that images are generated with prompts that are too short to represent a realistic description of a natural image. Another bias is due to the heterogeneity of VAEs that are used to decode the generated image from the latent to the pixel space. The training proposed in B-Free [13] used only natural images going to the VAE or inpainted images with StableDiffusion2 to produce a training database of AI-processed images treated as "generated" images. The original images come from the COCO database. For video detection [5], the frames of the generated class are also encoded by a VAE, and to improve generalization, the high-pass subbands of the original frames are injected in the encoded frames. A similar strategy [3] has recently been proposed by using JPEG compression as a calibration between original images and auto-encoded images, the calibrated auto-encoded images forming the class of generated images during training. Note that all three methods [5],[13] and [3] finetune DINOv2 [29] to train the classifier.

3 Methodology

3.1 ViT Classification

Vision Transformers have been widely adopted for various image classification tasks. In a nutshell, an input image $x \in \mathbb{R}^{H \times W \times C}$ is first split into non-overlapping patches of size $p \times p$, where each patch is further flattened to a vector $x_i^p \in \mathbb{R}^{p^2 C}$, $i = 1, \dots, N$, where $N = \frac{HW}{p^2}$ is the number of patches. Let us further denote $n = HW$, the number of pixels. Each patch is then linearly projected to a D -dimensional embedding

$$z_i^{(0)} = W_E x_i^p + b_E, \quad W_E \in \mathbb{R}^{D \times p^2 C}. \quad (1)$$

This is just a fully connected layer applied to each patch.

The embeddings are now stacked into a sequence $Z_0 = [z_1^{(0)}; \dots; z_N^{(0)}] \in \mathbb{R}^{N \times D}$. Since transformers don't know by default the positions of the patches, the positional encodings are simply added $Z_0 \leftarrow Z_0 + E_{pos}$, $E_{pos} \in \mathbb{R}^{N \times D}$.

A special learnable class token z_{cls} ([CLS]) is typically prepended and initialized randomly [9]. In addition, extra r learnable register tokens z_{R_1}, \dots, z_{R_r} , are often added as well [8], although recent work reports that the registers are not, in fact, needed during training [14]. The image is then represented by a sequence $Z_0 = [z_{cls}^{(0)}; z_{R_1}^{(0)}; \dots; z_{R_r}^{(0)}; z_1^{(0)}; \dots; z_N^{(0)}] \in \mathbb{R}^{(N+1+r) \times D}$.

The embeddings are then progressively updated using the transformer blocks, which can be expressed as:

$$\begin{aligned} Z' &= MSA(LN(Z_i)) + Z_i, \\ Z_{i+1} &= MLP(LN(Z')) + Z', \end{aligned} \quad (2)$$

where $LN(\cdot)$ is a Layer normalization, $MLP(\cdot)$ a 2-layer MLP with GELU/ReLU activation, and $MSA(\cdot)$ a Multi-head Self-Attention. For each head of the attention, we compute queries, keys, and values as $Q = ZW_Q$, $K = ZW_K$, and $V = ZW_V$, with $W_Q, W_K, W_V \in \mathbb{R}^{D \times d_k}$. The attention scores are computed as

$$A = \text{softmax}\left(\frac{QK^T}{\sqrt{d_k}}\right)V. \quad (3)$$

The multi-head attention with h heads uses a learnable matrix $W_O \in \mathbb{R}^{(h \cdot d_k) \times D}$ to output a combination of the attention scores $MSA(Z) = [A_1; \dots; A_h]W_O$.

After L layers of transformer blocks, the [CLS] token is used for prediction:

$$\hat{y} = \text{softmax}(W_{cls} z_{cls}^{(L)} + b_{cls}). \quad (4)$$

The prediction \hat{y} , together with true labels y , is then typically fed to a loss function, such as binary cross-entropy.

3.2 Bias-Free Training

To construct a lightweight detector of local manipulations, we leverage a backbone that has already been trained for generated content detection. We adopt the recent B-Free model [13], which builds upon a Vision Transformer (ViT) introduced in [8] with four registers ($r = 4$) and pre-trained using DINOv2 self-supervised learning [29]. The ViT operates on 504×504 images, employs a patch size of $p \times p = 14 \times 14$, an embedding dimension of $D = 768$, and consists of twelve multi-head self-attention layers with a head dimension $d_k = D/h = 64$. We refer to this backbone as DINOv2-B, reserving the name B-Free for the dataset.

The authors of B-Free generate forged images from authentic ones by applying Stable Diffusion 2 inpainting. Their key idea is to eliminate semantic bias in the training data by ensuring that both real and forged samples share identical background semantics, thereby compelling the model to learn to detect subtle artifacts introduced during inpainting rather than relying on high-level semantic cues. Experiments show that this training strategy yields strong generalization and robustness to a wide range of image generators and post-processing operations. We initialize our detector with the publicly available DINOv2-B weights, as described in the following section.

3.3 DinoLizer - ViT for Localization

Since the [CLS] token aggregates information from the entire image, it is unsuitable for pixel-level localization. Instead we focus on the patch embeddings (patch tokens) $[z_1^{(L)}; \dots; z_N^{(L)}]$, each of which encodes the visual content of its corresponding patch. To obtain a per-patch modification probability p_i , we attach a lightweight linear classification head to each embedding and apply the softmax:

$$p_i = \text{softmax}(W_{cls}z_i^{(L)} + b_{cls}), \quad i = 1, \dots, N, \quad (5)$$

where $W_{cls}z_i^{(L)} + b_{cls}$ is the i -th patch logit. This operation is equivalent to a 1×1 convolution applied to the patch tokens, as illustrated in Figure 1.

A similar strategy has previously been employed for semantic segmentation with Vision Transformers [29, 33]. After computing the patch-level probabilities, we upsample each p_i to pixel resolution by assigning its value to all $p \times p$ pixels within the corresponding patch. The segmentation head is trained with Dice Loss [25]:

$$\mathcal{L}_{Dice} = 1 - \frac{2 \sum_{i=1}^n p_i g_i + \epsilon}{\sum_{i=1}^n p_i^2 + \sum_{i=1}^n g_i^2 + \epsilon} \quad (6)$$

where $g_i \in \{0, 1\}$ denotes the ground-truth label for pixel i (1 = forged, 0 = pristine), and $\epsilon = 1$ is a small smoothing constant.

Unlike the training protocol of B-Free, we treat auto-encoded pixels as pristine rather than forged. This choice aligns with our application objective - detecting only generative alterations while ignoring artefacts introduced by auto-encoding. The ablation study in Section 5.2 confirms that this convention yields superior localization performance on average.

Finally, we optimise only the classification head defined in (5), which contains $D + 1 = 768$ learnable parameters, while keeping the ViT backbone frozen. This lightweight design results in a training time of merely 11h on a single NVIDIA Tesla V100 GPU, mainly due to the rather large training dataset.

Sliding-window Inference

To localize inpainted regions in images of arbitrary resolution, we avoid any down-sampling that could erode discriminative forensic cues. Instead, we apply a sliding window of size $w \times w = 504 \times 504$ with stride s to the input image, producing a set of overlapping patches. For each patch we compute logits via the linear classification head and then sum the logits over all windows that cover a given pixel. This procedure is equivalent to averaging the logits across overlapping windows, but because the decision threshold remains fixed at 0 (or 1/2 when working in probability space), a linear scaling of the logits does not alter the final classification. Figure 1 illustrates this sliding-window pipeline.

A grid search over stride values revealed that $s \in \{64, 128\}$ yields comparable localization performance, while $s = 128$ halves the number of windows and thus accelerates inference. Consequently we adopt $s = 128$ for all subsequent experiments. The window size w matches the spatial resolution of images in our training set (see Section 4.1).

We observed that multiple overlapping windows improve prediction quality. Hence, all small test images are upscaled to at least 1016×1016 pixels using bicubic interpolation, guaranteeing a 5×5 grid of windows for localization. This upscaling increases the diversity of crops prior to averaging, further enhancing the accuracy of the localization map. Mirror padding is applied when necessary to align the sliding windows with the image boundaries and the resulting masks are cropped back to the original image size.

Although our detector is built upon the DINOv2-B backbone, it departs fundamentally from its conventional use. Standard DINOv2-B evaluates five crops (four corners and the centre) from larger images and averages their probabilities to produce a single binary decision. When the inpainted region is small, this strategy often fails, as the overall image remains largely authentic. By contrast, our sliding-window approach yields a dense per-pixel pre-

Model	Byd the Brush		CocoGlide		TGIF		SAGI-FR		SAGI-SP		B-Free		Average	
	IOU	F1	IOU	F1	IOU	F1	IOU	F1	IOU	F1	IOU	F1	IOU	F1
DinoLizer (ours)	0.42	0.56	0.57	0.69	<u>0.39</u>	<u>0.49</u>	0.23	0.33	0.48	0.60	0.70	0.81	0.47	0.58
TruFor [12]	<u>0.22</u>	<u>0.30</u>	0.29	0.36	0.70	0.80	0.16	0.20	0.48	<u>0.55</u>	0.22	0.30	<u>0.35</u>	<u>0.42</u>
SAFIRE [19]	0.12	0.17	<u>0.40</u>	<u>0.47</u>	0.21	0.28	<u>0.21</u>	<u>0.28</u>	0.27	0.33	<u>0.24</u>	<u>0.32</u>	0.24	0.31
ManTra-Net [39]	0.06	0.10	0.26	0.35	0.26	0.35	0.02	0.03	0.27	0.35	0.05	0.08	0.15	0.21
CAT-Net v2 [18]	0.13	0.20	0.17	0.24	0.14	0.23	0.03	0.05	0.11	0.18	0.03	0.06	0.10	0.16
SparseViT [4]	0.05	0.08	0.32	0.39	0.11	0.15	0.09	0.11	0.12	0.15	0.13	0.17	0.14	0.18

Table 2: Average pixel-level IOU and F1 score comparison on image forgery localization. The best results are shown in bold, the second best are underlined.

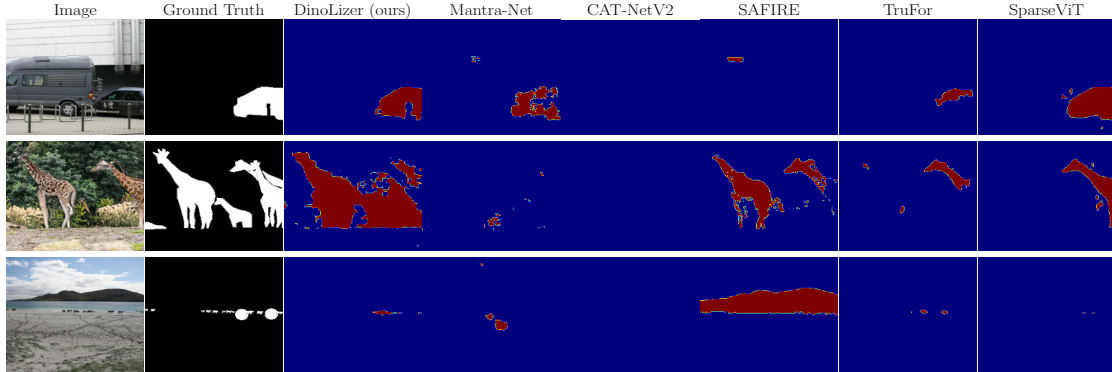


Figure 2: Visual comparison of forgery localization results on the CocoGlide dataset.

diction map that can reveal localized forgeries even when the global image statistics are unchanged.

4 Results

4.1 Experimental Setup

Training

We finetune our detector on the B-Free dataset [13], which contains 51k real and 309k synthetic images, each of size 512×512 . The real samples are drawn from MSCOCO [21], whereas the synthetic images are reconstructed and inpainted variants of these real images produced with Stable Diffusion 2.1. The dataset is split into 80% for training, 10% for validation and 10% for testing. For images with pristine backgrounds we assign the same ground-truth masks as those with forged backgrounds, since the background remains semantically identical. The data augmentation scheme (JPEG compression, double JPEG compression, cropping, resizing, blurring, color-jittering, additive noise, and their possible combination) together with the hyperparameter configuration are detailed in the supplementary materials.

Testing

We evaluate our method on 5 public datasets of generative inpainting. In particular, we use the inpainted images from B-Free [13] (our testing set), Beyond the Brush [1], CocoGlide [12], TGIF [24], SAGI-SP [11], and SAGI-FR [11]. The latter is derived from the SAGI benchmark but contains images whose background has been fully regenerated by the inpainting model. Across all datasets we consider roughly 25k, see the details on the datasets listed in Table 1. For every dataset we restrict our experiments to scenarios where the images are inpainted against pristine backgrounds, with the sole exception of SAGI-FR, which contains images with fully regenerated backgrounds.

Metrics

We use IOU (Intersection over Union) and F1 score as the metrics to evaluate the performance of our method. We use a fixed threshold of 0.5 to binarize the predicted mask. We consider IOU equal to 1 when both the predicted mask and the ground truth mask are empty (i.e., no forged pixels), which is necessary during training, as there are also fully pristine images. The metrics are computed

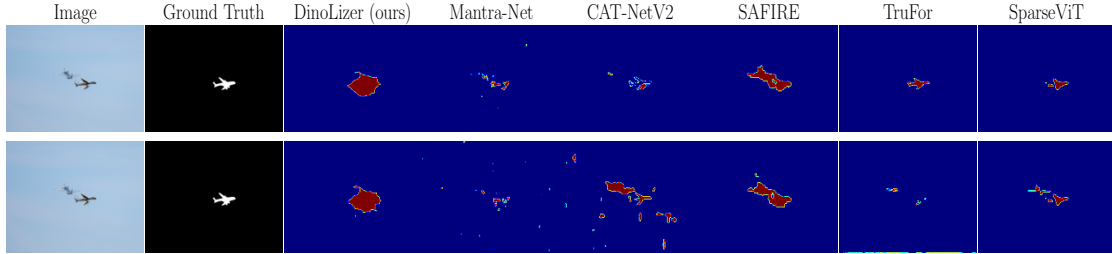


Figure 3: Visual comparison of forgery localization results on the TGIF dataset (top) and their JPEG QF 80 robustness (bottom).

as follows:

$$\text{IOU} = \frac{TP}{TP + FP + FN}, \quad (7)$$

$$\text{Precision} = \frac{TP}{TP + FP + \epsilon}, \quad (8)$$

$$\text{Recall} = \frac{TP}{TP + FN + \epsilon}, \quad (9)$$

$$\text{F1} = 2 \cdot \frac{\text{Precision} \cdot \text{Recall}}{\text{Precision} + \text{Recall} + \epsilon}, \quad (10)$$

where TP, FP, FN are the number of true positive, false positive, and false negative pixels, respectively ($\epsilon = 10^{-8}$ is a small constant to avoid division by zero).

4.2 State-of-the-art Comparison

We evaluate DinoLizer against a representative set of state-of-the-art inpainting-forgery detectors, employing only the publicly released weights. The competing methods are TruFor [12], SAFIRE [19], ManTra-Net [39], CAT-Net v2 [18], and SparseViT [4]. All models are used off-the-shelf without any additional re-training.

Table 2 summarizes the quantitative results. DinoLizer attains the highest F1 score across all datasets, with the sole exception of the TGIF benchmark where TruFor slightly surpasses it. On average, our approach outperforms the other detectors by at least 16% in F1.

Figure 2 presents a qualitative comparison of the predicted masks on the CocoGlide dataset. Additional visual examples for the remaining datasets are provided in the supplementary material.

After a careful inspection, we learned that the TGIF contains very fine-grained inpainting changes, which is very well captured by TruFor, but the DinoLizer tends to detect even its neighborhood due to the patch-based detection as manipulated, resulting in a loss of F1 score. However, in the presence of JPEG compression or other processing, TruFor’s detection deteriorates rapidly, while DinoLizer is very robust, see Figure 3 for a visual example. More robustness analysis and visual examples in TGIF are provided in the supplementary materials.

Robustness Evaluation

In this section we evaluate the robustness of the detectors against a variety of common post-processing operations. Four perturbation classes are considered:

- JPEG compression with quality factors $QF \in \{100, 80, 60, 40\}$,
- Double JPEG compression (first pass $QF_1 = 90$, second pass $QF_2 \in \{90, 60, 40\}$),
- Bicubic resizing to 50%, 150% and 200% of the original resolution,
- Additive Gaussian noise with standard deviations $\sigma \in \{3, 7, 15, 19\}$.

The resulting F1 scores on the CocoGlide and SAGI-SP benchmarks are plotted in Figure 4 and Figure 5, respectively. Across all perturbations, DinoLizer consistently outperforms the competing localizers, the only exception is the upsampling case on SAGI-SP, where TruFor achieves a marginally higher F1. DinoLizer’s performance remains relatively stable as the severity of compression, resizing and noise increases, an effect that we attribute to the training augmentations explicitly incorporating these operations. We find particularly interesting the contrast against the other ViT-based detector - SparseViT. Although its qualitative trends mirror those of DinoLizer, its F1 scores lag by 20-60%.

5 Ablation Studies

5.1 Classification Head

We now investigate different approaches to making predictions at the patch level. The naive idea would be to simply use the off-the-shelf DINOv2-B and use its last attention of the [CLS] token towards every patch to examine how the model focuses on different regions of the image when determining whether the image is generated or not. Let us denote $\alpha_i^{(m)}$ the m -th head’s last attention

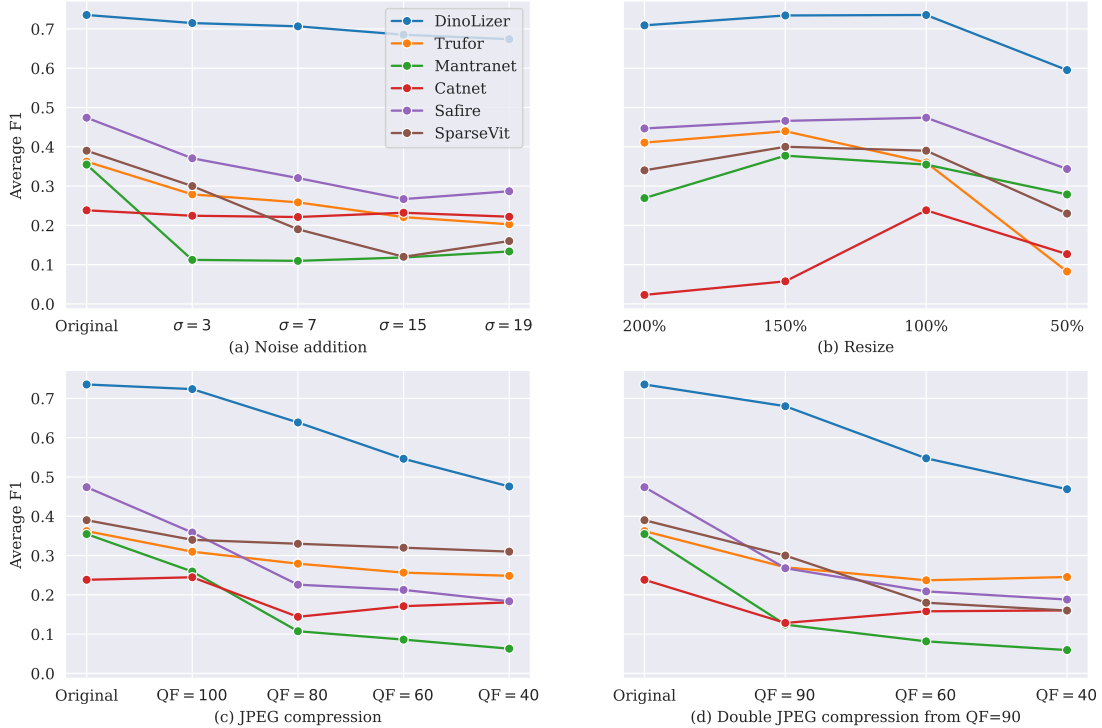


Figure 4: F1 score performance under different types of perturbations on CocoGlide: (a) gaussian noise, (b) resizing, (c) JPEG compression, and (d) double JPEG compression.

Strategy	Byd the Brush		CocoGlide		TGIF		SAGI-FR		SAGI-SP		B-Free		Average	
	IOU	F1	IOU	F1	IOU	F1	IOU	F1	IOU	F1	IOU	F1	IOU	F1
Avg Attention	0.33	0.48	0.41	0.55	0.26	0.38	0.22	0.32	0.35	0.48	0.61	0.74	0.36	0.49
Weighted Attention	0.35	0.49	0.43	0.56	0.27	0.39	0.21	0.31	0.36	0.49	0.61	0.74	0.37	0.50
Patch Embedding	0.42	0.56	<u>0.57</u>	<u>0.69</u>	0.39	0.49	0.23	0.33	0.48	0.60	<u>0.70</u>	<u>0.81</u>	<u>0.47</u>	<u>0.58</u>
Patch Embedding (MLP)	0.41	0.56	0.59	0.72	0.37	0.47	0.24	0.35	0.48	0.59	0.76	0.85	0.48	0.59
Patch Embedding (504)	0.31	0.42	0.56	0.69	0.27	0.35	0.26	0.36	0.44	0.55	0.68	0.78	0.42	0.53
Patch Emb (VAE as fake)	0.35	0.47	0.40	0.51	0.20	0.28	0.21	0.30	0.30	0.40	0.67	0.78	0.36	0.46

Table 3: Attention is not all you need: comparison of different Dinov2 strategies for image forgery localization using IOU and F1 scores.

$A_{0,5+i}^{(L-1)}$ (we skip attention for [CLS] and 4 registers) towards i -th patch, $m = 1, \dots, h$, $i = 1, \dots, N$.

First, we simply average the attentions over all $h = 12$ attention heads $\bar{\alpha}_i = \frac{1}{h} \sum_{m=1}^h \alpha_i^{(m)}$. This strategy does not involve any optimization. Secondly, we learn weights w_m , $m = 1, \dots, h$ to minimize the Dice loss (6) while using weighted attentions $\alpha_i^{(w)} = \sum_{m=1}^h w_m \alpha_i^{(m)}$ (scaled to 0-1 range) as inputs. Due to its simplicity, we use only 100 randomly selected images from the B-Free dataset for the training. As we can see in Table 3, using the weighted strategy helps, although the results are not much different, since we only optimize 12 parameters. Next, we test the approach proposed in Section 3.3 using the patch embeddings $[z_1^{(L)}; \dots; z_N^{(L)}]$ with retraining the classification head. We can see a clear improvement in every tested

scenario, which is why this strategy has been selected for DinoLizer.

We further expanded the head into a 2-layer MLP with a hidden layer of size $D = 768$. As we can see, the results are not much better with extra computational overhead.

Since we resize testing images to a size of at least 1016×1016 , we additionally verify testing potentially smaller images (504×504), which provides even faster inference. However, due to having only 1 sliding window per image of this size, the results are less promising.

5.2 Class of Auto-encoded Patches

We also investigated a variant of the training protocol in which the regenerated background - i.e. pixels that pass

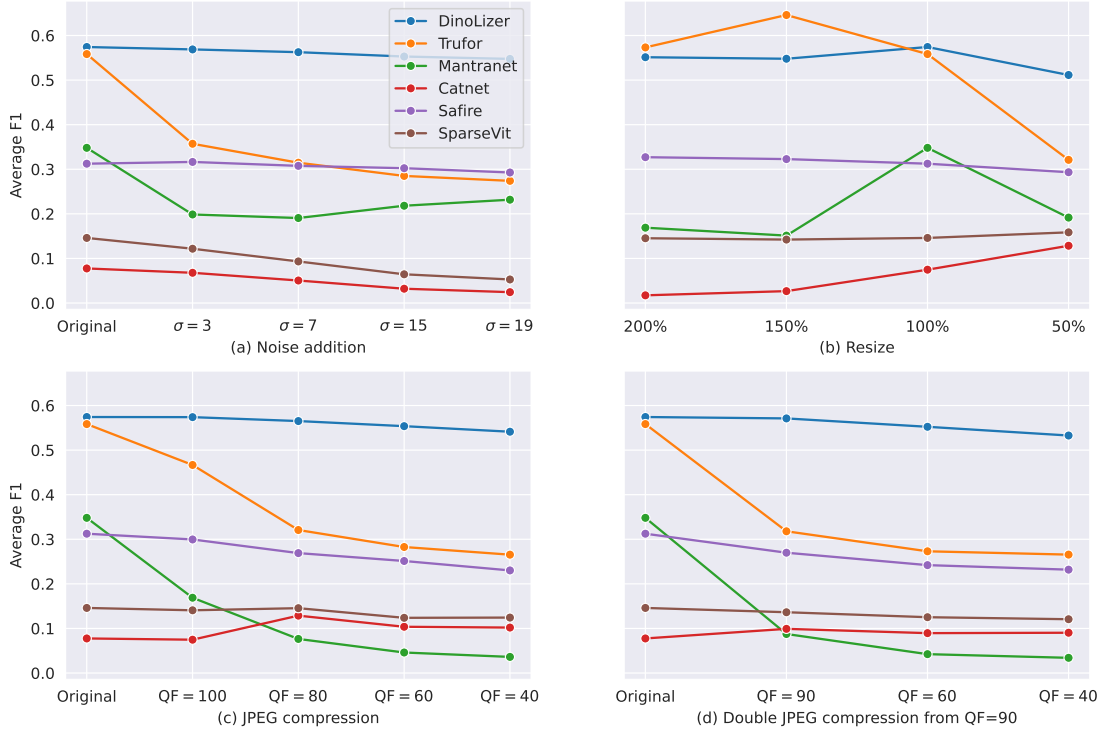


Figure 5: F1 score performance under different types of perturbations on SAGI-SP: (a) gaussian noise, (b) resizing, (c) JPEG compression, and (d) double JPEG compression.

through the VAE but are not semantically altered - is labeled as fake. This modification yields a modest improvement on the B-Free training set, but it degrades performance on every other dataset. We attribute this drop to over-fitting on artefacts introduced by the VAE employed in B-Free.

5.3 Architecture

In the following experiment we investigate how the choice of ViT backbone and the decision to freeze or finetune it affect localization performance. We evaluate three backbones: **DINOv2** [29]: a ViT-B/14 architecture distilled with register tokens, comprising 86M parameters – **DINOv2-B** [13]: the same backbone further finetuned on the B-Free dataset – **DINOv3** [32]: a ViT-B/16 distilled model with 86M parameters.

For each backbone we consider two training regimes:

(1): **Frozen encoder + linear head**: only a linear classification head is learned, as commonly adopted in recent literature [6, 28], – (2): **End-to-end (e2e) finetuning**: the entire network is updated during training.

Additionally, we evaluate a third configuration for DINOv2-B in which all weights are kept frozen and its classification head trained on the [CLS] token is used on the patch embeddings. Table 4 demonstrates that this

frozen-head strategy yields unsatisfactory localization results.

Table 4 reveals several noteworthy trends. First, end-to-end finetuning produces a pronounced improvement on the B-Free training set but fails to generalize well to other datasets. Second, the extra pretraining of DINOv2-B offers only a modest advantage over the base DINOv2 model, indicating that the backbone already encodes substantial localization-relevant information, an observation consistent with prior forensic work on specialized pre-training [2]. Finally, when only the linear head is trained, DINOv2 outperforms DINOv3. Conversely, in an end-to-end setting, DINOv3 exhibits a clear advantage. This suggests that the pretrained feature representations of DINOv3 are less aligned with the requirements of inpainting forgery localization than those of DINOv2.

6 Conclusion

Our work introduces a novel framework that utilizes the versatile DINO family of Vision Transformers to localize generated image regions with state-of-the-art performance across multiple benchmarks. The methodology fundamentally addresses the semantic challenge in inpainting forgeries by explicitly modeling auto-encoded regions as

Model	Training	Byd the Brush		CocoGlide		TGIF		SAGI-FR		SAGI-SP		B-Free		Average	
		IOU	F1	IOU	F1	IOU	F1	IOU	F1	IOU	F1	IOU	F1	IOU	F1
DINOv2-B [13]	-	0.08	0.14	0.11	0.19	0.03	0.06	0.12	0.18	0.12	0.19	0.19	0.29	0.11	0.18
DINOv2-B	head	0.42	0.56	0.57	0.69	0.39	0.49	<u>0.23</u>	<u>0.33</u>	0.48	0.60	0.70	0.81	0.47	0.58
DINOv2	head	<u>0.37</u>	<u>0.51</u>	<u>0.55</u>	<u>0.68</u>	<u>0.36</u>	<u>0.47</u>	0.23	0.33	<u>0.44</u>	<u>0.56</u>	0.62	0.74	<u>0.43</u>	<u>0.55</u>
DINOv3	head	0.19	0.28	0.47	0.58	0.24	0.33	0.30	0.41	0.37	0.50	0.47	0.59	0.34	0.45
DINOv2-B	e2e	0.02	0.04	0.17	0.21	0.26	0.32	0.15	0.22	0.22	0.28	<u>0.81</u>	<u>0.88</u>	0.27	0.33
DINOv2	e2e	0.03	0.04	0.14	0.17	0.24	0.30	0.16	0.22	0.20	0.26	0.78	0.86	0.26	0.31
DINOv3	e2e	0.09	0.12	0.28	0.34	0.32	0.38	0.23	0.31	0.32	0.39	0.89	0.94	0.36	0.41
TruFor [12]	-	0.22	0.30	0.29	0.36	0.70	0.80	0.16	0.20	0.48	0.55	0.22	0.30	0.35	0.42
SAFIRE[19]	-	0.12	0.17	0.40	0.47	0.21	0.28	0.21	0.28	0.27	0.33	0.24	0.32	0.24	0.31

Table 4: Performance metrics across datasets by training only the head or the whole model end-to-end (e2e). Comparison between DINOv3, DINOv2, and B-Free-pretrained DINOv2-B. Best results are in bold, and the second best are underlined.

semantically preserved, thereby avoiding semantic biases that are detrimental to localization systems. The solution demonstrates computational efficiency: by leveraging DINO’s patch tokens and employing a sliding window approach, we maintain operations that require only a single GPU for both training and inference, even with large images. Furthermore, our comprehensive data augmentation strategy ensures robust performance against typical image post-processing operations, including noise addition, resizing, and JPEG (double) compression. This resilience is particularly valuable considering the varied processing pipelines that forgeries may undergo before analysis. Importantly, this framework shows strong potential for adaptation to future vision transformer architectures. Its success with both DINOv2 and the emerging DINOv3 suggests that this methodology can scale alongside advancements in generative models.

Supplementary Document

A Implementation Details

As outlined in Section 5.3, DinoLizer is based on a ViT-B/14 backbone with registers, refined on the B-Free dataset [13]. To train its linear classification head we adopted the following hyper-parameter configuration:

- batch size: 64,
- initial learning rate: 10^{-3} ,
- learning rate scheduler: `lrdrop` decreasing the learning rate by half whenever the validation loss does not improve for four consecutive epochs,
- optimizer: `adamW`,
- weight decay: 10^{-5} .

The training was capped at 100 epochs, with early stopping triggered once the learning rate fell below 10^{-6} . The best validation performance was achieved after 15 epochs with each epoch lasting 42 minutes on a single NVIDIA V100 GPU with 32GB of memory.

Augmentations

To robustify the detector against common image processing operations, while still training on images of size $H \times W = 504 \times 504$, we used the following combination of augmentations implemented with the Albumentations library (<https://albumentations.ai/>):

- Random horizontal flip with probability 0.5 ($p = 0.5$),
- Random rotation by 90° ($p = 1$),
- One of the following, each with $p = 0.25$:
 1. `RandomResizedCrop` to size $H \times W$ with a scale factor uniformly sampled from $(0.1, 1)$ and aspect ratio fixed at 1,
 2. `RandomCrop` to size $H \times W$,
 3. Resizing directly to size $H \times W$,
 4. Upscaling by either 200% or 300%, followed by `RandomCrop` to size $H \times W$,
- Uniform box blur with kernel size $k \in \{3, 4, 5\}$ ($p = 0.1$),
- Gaussian noise with standard deviation σ uniformly sampled from $(0.2, 0.44)$ ($p = 0.1$),
- Color jitter ($p = 0.1$),

Dataset	min-max H	min-max W	mask size \bar{m}	\bar{m}_W
BtB [1]	234 – 1152	246 – 1152	0.22	0.27
B-Free [13]	512	512	0.47	0.59
COCOG [12]	256	256	0.25	0.32
TGIF [24]	518 – 1024	539 – 1024	0.06	0.12
SAGI- SP [11]	144 – 4928	200 – 4928	0.19	0.31
FR [11]	139 – 2048	216 – 2048	0.20	0.27

Table 5: Overview of evaluation datasets with their image sizes (H - height range, W - width range), their average relative mask size \bar{m} , and average mask size \bar{m}_W per overlapping (modified) windows of size 504×504 with stride $S = 128$.

- First JPEG compression with quality factor QF uniformly drawn from $\{40, \dots, 100\}$ ($p = 0.5$),
- Optional second JPEG compression with quality factor QF_2 drawn from $\{40, \dots, 100\}$ ($p = 0.1$ if first compression applied).

All resizing operations employ Lanczos interpolation.

During validation, we accelerate the evaluation by applying only a center crop followed by JPEG compression with a randomly selected quality factor between 40 and 100, applied with probability $p = 0.5$.

B Qualitative Study

To assess the robustness of our method, we evaluated its performance on several out-of-distribution datasets that were not included in the training set, as described in Section 4.1. These datasets differ both in their image sources and the generative models employed (see Table 1) and exhibit a wide range of image dimensions (Table 5). In the following analysis, we focus on two datasets, TGIF and SAGI-FR, in which DinoLizer’s performance appears suboptimal.

Failure case of TGIF

To understand why DinoLizer exhibits inferior performance on the TGIF dataset relative to TruFor, we analyzed the distribution of modification sizes within images. For each image (after a possible upsampling required for small inputs, as described in Section 3.3), we computed the mean mask size over overlapping sliding windows of 504×504 pixels with stride $S = 128$, restricting the analysis to windows that contain at least one modified pixel. This metric reflects the typical size of alterations that DinoLizer is expected to detect within each image. We denote the mean mask size for the i -th image as $m_W^{(i)}$, and

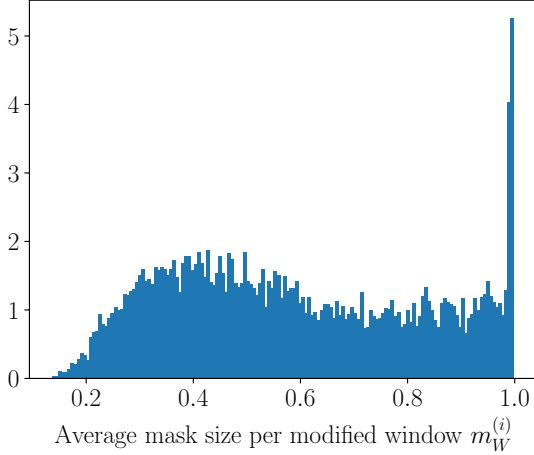


Figure 6: Histogram of average changes per modified overlapping windows of size 504×504 with stride 128 ($m_W^{(i)}$) in B-Free dataset.

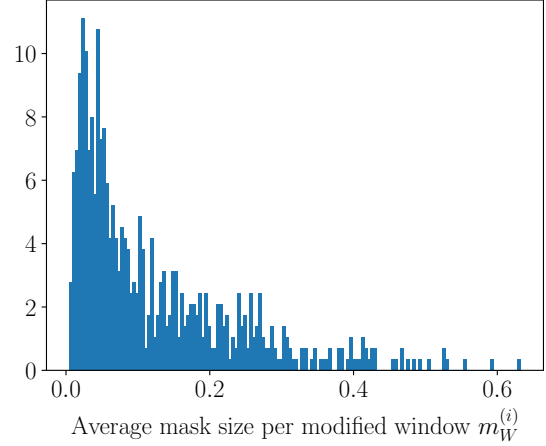


Figure 7: Histogram of average changes per modified overlapping windows of size 504×504 with stride 128 ($m_W^{(i)}$) in TGIF dataset.

its average over a dataset as \bar{m}_W , which is reported in the last column of Table 5.

In the B-Free dataset (used for training) we observe that, on average, 59% of the pixels in each modified window are altered. The discrepancy with the overall average mask size \bar{m} of 47% arises because \bar{m} is computed over the images without upsampling small images and includes both modified and unmodified regions, whereas \bar{m}_W focuses exclusively on windows containing modifications.

Table 5 also shows that \bar{m}_W for TGIF is only 12%. Figure 6 demonstrates that nearly all B-Free images have $m_W^{(i)}$ exceeding 12%, whereas Figure 7 indicates that most TGIF images exhibit $m_W^{(i)}$ below 12%. Consequently, DinoLizer is ill-suited for detecting manipulations that occupy relatively small portions of an image (roughly 20% of a 504×504 window, corresponding to 225×225 pixels or smaller). This limitation is further illustrated by the last visual example in Figure 13, where a small modified region is missed. Note that the images in the visual example are scaled for better visualization and the last example is indeed smaller than the others. A straightforward remedy could be to augment the training set with small manipulated regions, but we were unable to implement this improvement in the current manuscript due to time constraints.

Failure case of SAGI-FR

As we see in Table 2, DinoLizer’s performance decreases markedly when evaluated on the SAGI-FR dataset relative to SAGI-SP. The model is trained to classify content reconstructed by a VAE (without inpainting) as authentic, and we hypothesize that this training regime ex-

plains the observed drop. According to Table 1, the inpainting procedure employed in SAGI-FR relies on different generative models than Stable Diffusion 2 used in the B-Free dataset. Consequently, DinoLizer tends to interpret the reconstructed background in SAGI-FR images as inpainted artefacts. This behavior is corroborated by Figure 10, where DinoLizer (along with several other detectors) achieves higher F1 scores as the strength of post-processing increases and high-frequency traces introduced by the VAE are progressively attenuated. Further visual evidence is presented in Figure 14.

C Additional Robustness Results

To provide a comprehensive assessment of the robustness of our proposed localizer, we present F1-score curves for the four missing benchmark datasets missing in the main part of the paper: Beyond the Brush (Figure 8), TGIF (Figure 9), SAGI-FR (Figure 10), and B-Free (Figure 11). Across these datasets, the trends mirror those observed for CocoGlide and SAGI-SP in Section 4.2: DinoLizer maintains a relatively stable performance across varying degrees of post-processing, consistently achieving higher F1 scores than competing detectors.

The only notable deviations appear on TGIF, where TruFor outperforms DinoLizer on unprocessed images, and on SAGI-FR, where DinoLizer (along with other detectors) benefits from more aggressive post-processing. These deviations are consistent with the explanations provided in the preceding section.

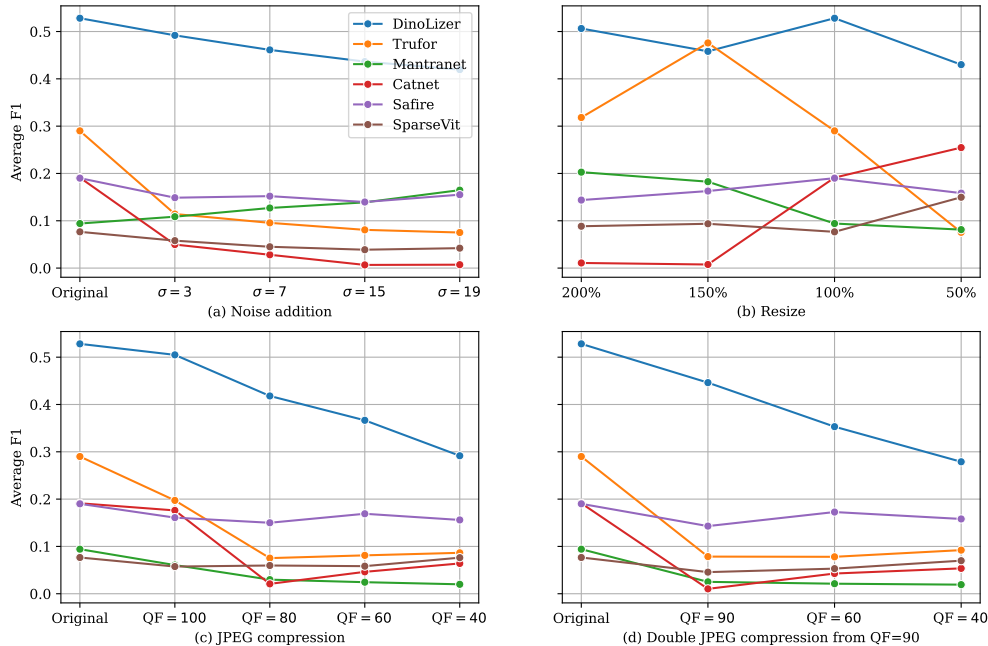


Figure 8: F1 score performance under different types of perturbations on Beyond the Brush: (a) gaussian noise, (b) resizing, (c) JPEG compression, and (d) double JPEG compression.

D Additional Visual Results

For completeness, we provide visual examples of predictions on additional datasets: Beyond the Brush (Figure 12), TGIF (Figure 13), SAGI-FR (Figure 14), SAGI-SP (Figure 15), and B-Free (Figure 16).

References

- [1] Giulia Bertazzini, Chiara Albisani, Daniele Baracchi, Dasara Shulani, and Alessandro Piva. Beyond the brush: Fully-automated crafting of realistic inpainted images. In *2024 IEEE International Workshop on Information Forensics and Security (WIFS)*, pages 1–6, 2024. 2, 5, 1
- [2] Jan Butora, Yassine Yousfi, and Jessica Fridrich. How to pretrain for steganalysis. page 143–148, New York, NY, USA, 2021. Association for Computing Machinery. 8
- [3] Ruoxin Chen, Junwei Xi, Zhiyuan Yan, Ke-Yue Zhang, Shuang Wu, Jingyi Xie, Xu Chen, Lei Xu, Isabel Guan, Taiping Yao, et al. Dual data alignment makes ai-generated image detector easier generalizable. *arXiv preprint arXiv:2505.14359*, 2025. 3
- [4] Xuanyao Chen, Zhijian Liu, Haotian Tang, Li Yi, Hang Zhao, and Song Han. Sparsevit: Revisiting activation sparsity for efficient high-resolution vision transformer. In *Proceedings of the IEEE/CVF Conference on Computer Vision and Pattern Recognition*, pages 2061–2070, 2023. 2, 5, 6
- [5] Riccardo Corvi, Davide Cozzolino, Ekta Prashnani, Shalini De Mello, Koki Nagano, and Luisa Verdoliva. Seeing what matters: Generalizable ai-generated video detection with forensic-oriented augmentation. *arXiv preprint arXiv:2506.16802*, 2025. 3
- [6] Davide Cozzolino, Giovanni Poggi, Riccardo Corvi, Matthias Nießner, and Luisa Verdoliva. Raising the bar of ai-generated image detection with clip. In *Proceedings of the IEEE/CVF Conference on Computer Vision and Pattern Recognition (CVPR)*, pages 4356–4366, 2024. 2, 8
- [7] Duc-Tien Dang-Nguyen, Cecilia Pasquini, Valentina Conotter, and Giulia Boato. Raise: a raw images dataset for digital image forensics. In *Proceedings of the 6th ACM Multimedia Systems Conference*, page 219–224, New York, NY, USA, 2015. Association for Computing Machinery. 2
- [8] Timothée Darcet, Maxime Oquab, Julien Mairal, and Piotr Bojanowski. Vision transformers need registers. In *The Twelfth International Conference on Learning Representations (ICLR)*, 2024. 3, 4
- [9] Jacob Devlin, Ming-Wei Chang, Kenton Lee, and Kristina Toutanova. Bert: Pre-training of deep bidirectional transformers for language understanding. In *Proceedings of the 2019 conference of the North American chapter of the association for computational linguistics: Human Language Technologies, Volume 1 (Long and Short Papers)*, pages 4171–4186, 2019. 3
- [10] Joel Frank, Thorsten Eisenhofer, Lea Schönherr, Asja Fischer, Dorothea Kolossa, and Thorsten Holz. Leveraging frequency analysis for deep fake image recognition. In *International conference on machine learning*, pages 3247–3258. PMLR, 2020. 2
- [11] Paschalis Giakoumoglou, Dimitrios Karageorgiou, Symeon Papadopoulos, and Panagiotis C Petrantonakis. Sagi: Semantically aligned and uncertainty guided ai image inpainting. In *International Conference on Computer Vision (ICCV)*, 2025. 2, 5, 1
- [12] Fabrizio Guillaro, Davide Cozzolino, Avneesh Sud, Nicholas Dufour, and Luisa Verdoliva. Trufor: Leveraging all-round clues for

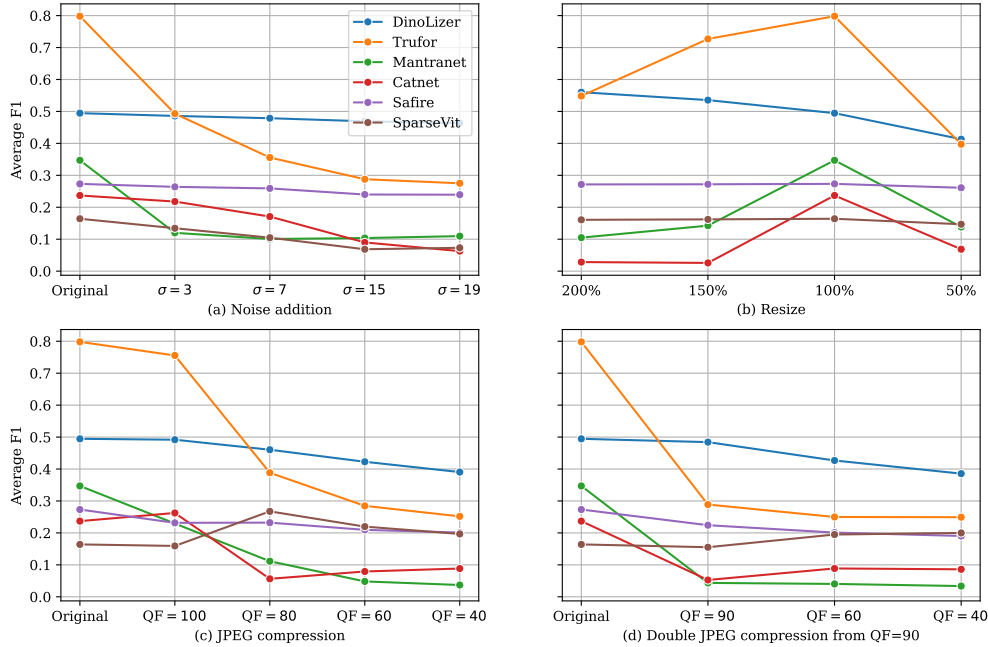


Figure 9: F1 score performance under different types of perturbations on TGIF: (a) gaussian noise, (b) resizing, (c) JPEG compression, and (d) double JPEG compression.

- trustworthy image forgery detection and localization. In *Proceedings of the IEEE/CVF conference on computer vision and pattern recognition (CVPR)*, pages 20606–20615, 2023. 2, 5, 6, 9, 1
- [13] Fabrizio Guillaro, Giada Zingarini, Ben Usman, Avneesh Sud, Davide Cozzolino, and Luisa Verdoliva. A bias-free training paradigm for more general ai-generated image detection. In *Proceedings of the Computer Vision and Pattern Recognition Conference (CVPR)*, pages 18685–18694, 2025. 2, 3, 4, 5, 8, 9, 1
- [14] Nick Jiang, Amil Dravid, Alexei Efros, and Yossi Gandelsman. Vision transformers don’t need trained registers. *arXiv preprint arXiv:2506.08010*, 2025. 3
- [15] Xuan Ju, Xian Liu, Xintao Wang, Yuxuan Bian, Ying Shan, and Qiang Xu. Brushnet: A plug-and-play image inpainting model with decomposed dual-branch diffusion. In *European Conference on Computer Vision*, pages 150–168. Springer, 2024. 2
- [16] Matthias Kirchner and Rainer Bohme. Hiding traces of resampling in digital images. *IEEE Transactions on Information Forensics and Security*, 3(4):582–592, 2008. 2
- [17] Alina Kuznetsova, Hassan Rom, Neil Alldrin, Jasper Uijlings, Ivan Krasin, Jordi Pont-Tuset, Shahab Kamali, Stefan Popov, Matteo Mallocci, Alexander Kolesnikov, et al. The open images dataset v4: Unified image classification, object detection, and visual relationship detection at scale. *International journal of computer vision*, 128(7):1956–1981, 2020. 2
- [18] Myung-Joon Kwon, Seung-Hun Nam, In-Jae Yu, Heung-Kyu Lee, and Changick Kim. Learning jpeg compression artifacts for image manipulation detection and localization. *International Journal of Computer Vision*, 130(8):1875–1895, 2022. 2, 5, 6
- [19] Myung-Joon Kwon, Wonjun Lee, Seung-Hun Nam, Minji Son, and Changick Kim. Safire: Segment any forged image region. pages 4437–4445, 2025. 2, 5, 6, 9
- [20] Yanhao Li, Quentin Bammey, Marina Gardella, Tina Nikoukhah, Jean-Michel Morel, Miguel Colom, and Rafael Grompone Von Gioi. Masksim: Detection of synthetic images by masked spectrum similarity analysis. In *Proceedings of the IEEE/CVF Conference on Computer Vision and Pattern Recognition*, pages 3855–3865, 2024. 2
- [21] Tsung-Yi Lin, Michael Maire, Serge Belongie, James Hays, Pietro Perona, Deva Ramanan, Piotr Dollár, and C. Lawrence Zitnick. Microsoft coco: Common objects in context. In *Computer Vision – ECCV 2014*, pages 740–755, Cham, 2014. Springer International Publishing. 2, 5
- [22] Antoine Mallet, Arthur Méreur, Minoru Kuribayashi, Rémi Coganne, and Patrick Bas. Simple detection of ai-generated images based on noise correlation. In *International conference on Advanced Machine Learning and Data Science (AMLDS) 2025*, 2025. 2
- [23] Hayk Manukyan, Andranik Sargsyan, Barsegh Atanyan, Zhangyang Wang, Shant Navasardyan, and Humphrey Shi. Hd-painter: high-resolution and prompt-faithful text-guided image inpainting with diffusion models. In *The Thirteenth International Conference on Learning Representations (ICLR)*, 2023. 2
- [24] Hannes Mareen, Dimitrios Karageorgiou, Glenn Van Wallendael, Peter Lambert, and Symeon Papadopoulos. Tgif: Text-guided inpainting forgery dataset. In *2024 IEEE International Workshop on Information Forensics and Security (WIFS)*, pages 1–6, 2024. 2, 5, 1
- [25] Fausto Milletari, Nassir Navab, and Seyed-Ahmad Ahmadi. V-net: Fully convolutional neural networks for volumetric medical image segmentation. In *2016 fourth international conference on 3D vision (3DV)*, pages 565–571. Ieee, 2016. 4

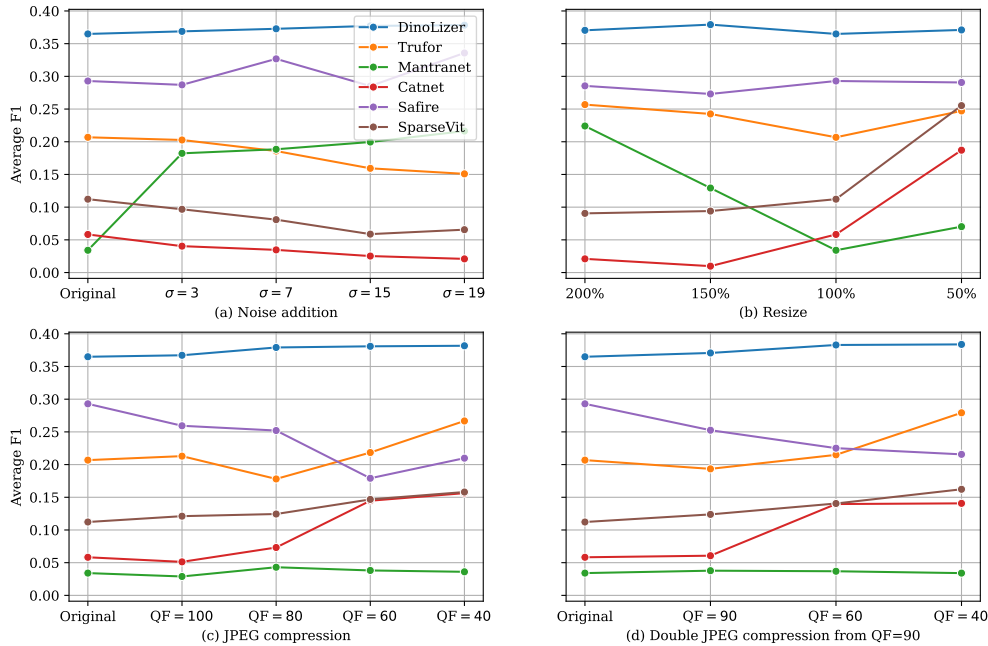


Figure 10: F1 score performance under different types of perturbations on SAGI-FR: (a) gaussian noise, (b) resizing, (c) JPEG compression, and (d) double JPEG compression.

- [26] Alex Nichol, Prafulla Dhariwal, Aditya Ramesh, Pranav Shyam, Pamela Mishkin, Bob McGrew, Ilya Sutskever, and Mark Chen. Glide: Towards photorealistic image generation and editing with text-guided diffusion models. *arXiv preprint arXiv:2112.10741*, 2021. 2
- [27] Alexander Quinn Nichol, Prafulla Dhariwal, Aditya Ramesh, Pranav Shyam, Pamela Mishkin, Bob McGrew, Ilya Sutskever, and Mark Chen. GLIDE: Towards photorealistic image generation and editing with text-guided diffusion models. In *Proceedings of the 39th International Conference on Machine Learning*, pages 16784–16804. PMLR, 2022. 2
- [28] Utkarsh Ojha, Yuheng Li, and Yong Jae Lee. Towards universal fake image detectors that generalize across generative models. In *Proceedings of the IEEE/CVF Conference on Computer Vision and Pattern Recognition (CVPR)*, pages 24480–24489, 2023. 2, 8
- [29] Maxime Oquab, Timothée Darcet, Théo Moutakanni, Huy Vo, Marc Szafraniec, Vasil Khalidov, Pierre Fernandez, Daniel Haziza, Francisco Massa, Alaaeldin El-Nouby, et al. Dinov2: Learning robust visual features without supervision. *Transactions on Machine Learning Research Journal*, pages 1–31, 2024. 3, 4, 8
- [30] Alec Radford, Jong Wook Kim, Chris Hallacy, Aditya Ramesh, Gabriel Goh, Sandhini Agarwal, Girish Sastry, Amanda Askell, Pamela Mishkin, Jack Clark, et al. Learning transferable visual models from natural language supervision. In *International conference on machine learning*, pages 8748–8763. PmlR, 2021. 2
- [31] Robin Rombach, Andreas Blattmann, Dominik Lorenz, Patrick Esser, and Björn Ommer. High-resolution image synthesis with latent diffusion models. In *Proceedings of the IEEE/CVF conference on computer vision and pattern recognition (CVPR)*, pages 10684–10695, 2022. 2
- [32] Oriane Siméoni, Huy V Vo, Maximilian Seitzer, Federico Baldassarre, Maxime Oquab, Cijo Jose, Vasil Khalidov, Marc Szafraniec, Seungeun Yi, Michaël Ramamonjisoa, et al. Dinov3. *arXiv preprint arXiv:2508.10104*, 2025. 8
- [33] Robin Strudel, Ricardo Garcia, Ivan Laptev, and Cordelia Schmid. Segmenter: Transformer for semantic segmentation. In *Proceedings of the IEEE/CVF international conference on computer vision (ICCV)*, pages 7262–7272, 2021. 3, 4
- [34] Lei Su, Xiaochen Ma, Xuekang Zhu, Chaoqun Niu, Zeyu Lei, and Ji-Zhe Zhou. Can we get rid of handcrafted feature extractors? sparsevit: Nonsemantics-centered, parameter-efficient image manipulation localization through spare-coding transformer. In *Proceedings of the AAAI Conference on Artificial Intelligence*, pages 7024–7032, 2025. 2, 3
- [35] Roman Suvorov, Elizaveta Logacheva, Anton Mashikhin, Anastasia Remizova, Arsenii Ashukha, Aleksei Silvestrov, Naejin Kong, Harshith Goka, Kiwoong Park, and Victor Lempitsky. Resolution-robust large mask inpainting with fourier convolutions. In *Proceedings of the IEEE/CVF winter conference on applications of computer vision*, pages 2149–2159, 2022. 2
- [36] Lea Uhlenbrock, Davide Cozzolino, Denise Moussa, Luisa Verdoliva, and Christian Riess. Did you note my palette? unveiling synthetic images through color statistics. In *Proceedings of the 2024 ACM Workshop on Information Hiding and Multimedia Security*, pages 47–52, 2024. 2
- [37] Sheng-Yu Wang, Oliver Wang, Richard Zhang, Andrew Owens, and Alexei A Efros. Cnn-generated images are surprisingly easy to spot... for now. In *Proceedings of the IEEE/CVF conference on computer vision and pattern recognition*, pages 8695–8704, 2020. 2
- [38] Shaoan Xie, Zhifei Zhang, Zhe Lin, Tobias Hinz, and Kun Zhang. Smartbrush: Text and shape guided object inpainting with diffusion model. In *Proceedings of the IEEE/CVF conference on com-*

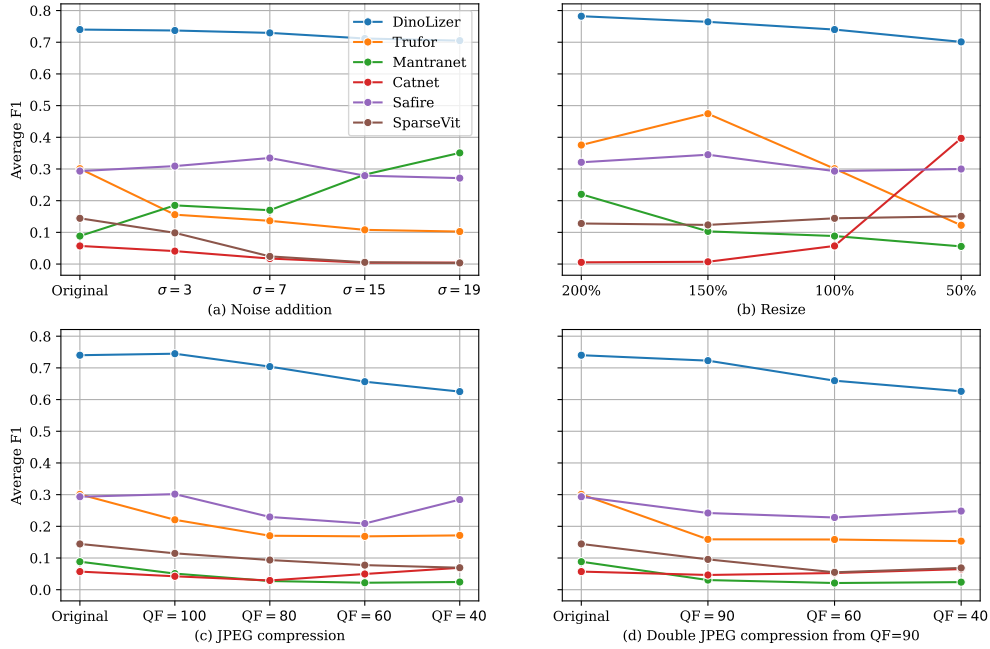


Figure 11: F1 score performance under different types of perturbations on B-Free: (a) gaussian noise, (b) resizing, (c) JPEG compression, and (d) double JPEG compression.

puter vision and pattern recognition, pages 22428–22437, 2023. 2

- [39] Wael AbdAlmageed Yue Wu and Premkumar Natarajan. Mantranet: Manipulation tracing network for detection and localization of image forgeries with anomalous features. In *The IEEE Conference on Computer Vision and Pattern Recognition (CVPR)*, 2019. 2, 5, 6
- [40] L. Zhang. Fooocus. <https://github.com/lillyasviel/Fooocus>, 2023. Online; accessed 2025-11-11. 2
- [41] Lvmin Zhang, Anyi Rao, and Maneesh Agrawala. Adding conditional control to text-to-image diffusion models. In *Proceedings of the IEEE/CVF international conference on computer vision (ICCV)*, pages 3836–3847, 2023. 2
- [42] Junhao Zhuang, Yanhong Zeng, Wenran Liu, Chun Yuan, and Kai Chen. A task is worth one word: Learning with task prompts for high-quality versatile image inpainting. In *European Conference on Computer Vision*, pages 195–211. Springer, 2024. 2

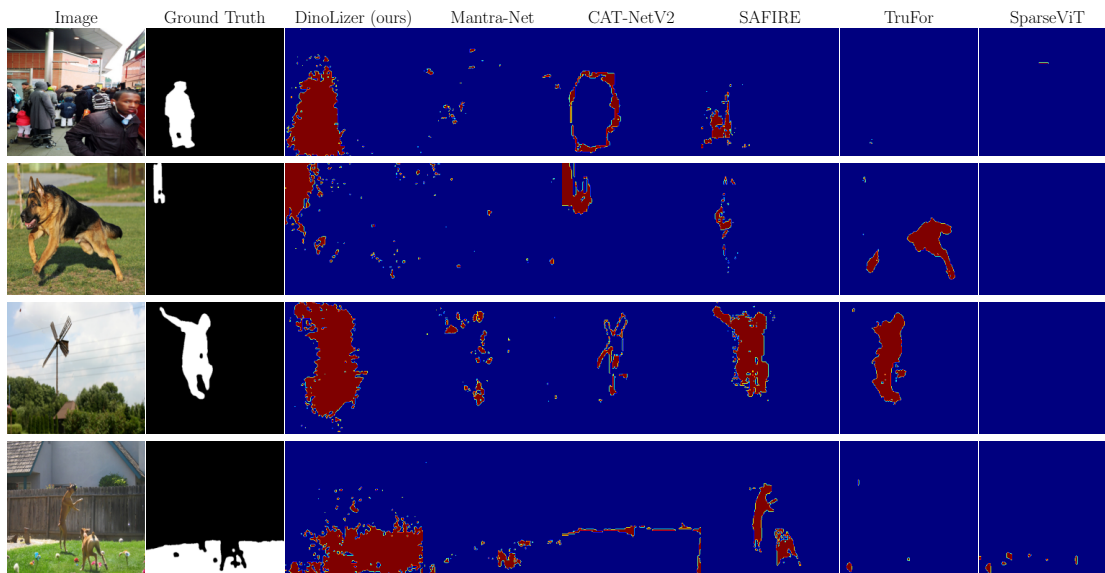


Figure 12: Visual comparison of forgery localization results on the Beyond the Brush dataset.

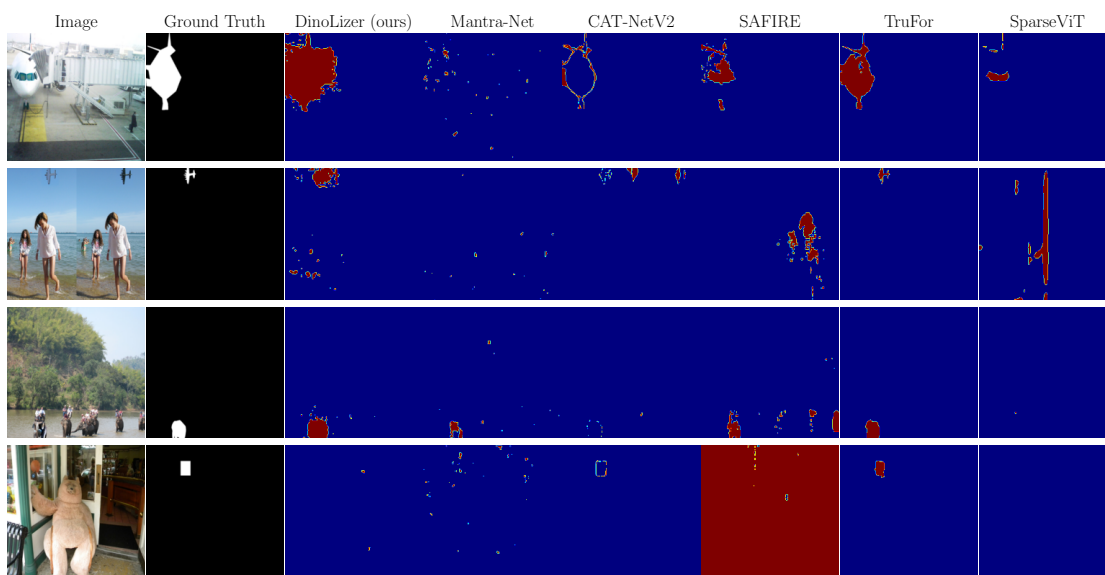


Figure 13: Visual comparison of forgery localization results on the TGIF dataset.

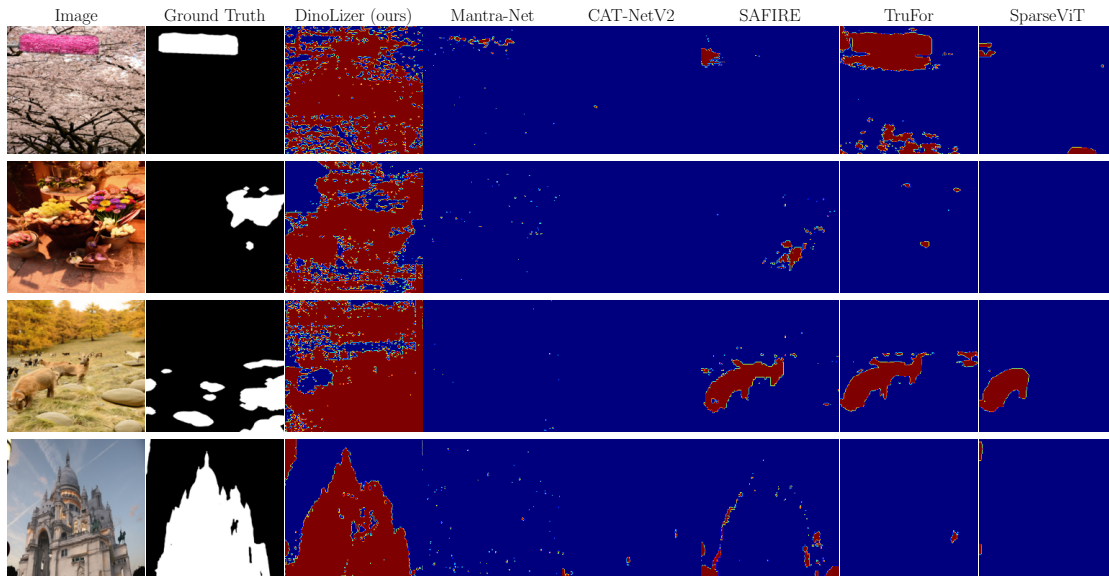


Figure 14: Visual comparison of forgery localization results on the SAGI-FR dataset.

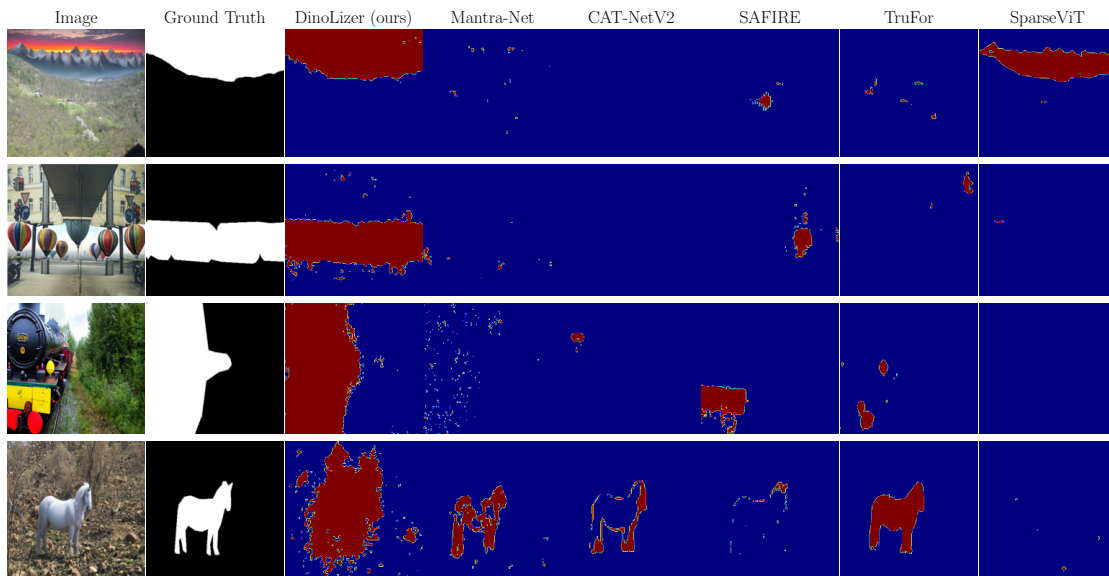


Figure 15: Visual comparison of forgery localization results on the SAGI-SP dataset.

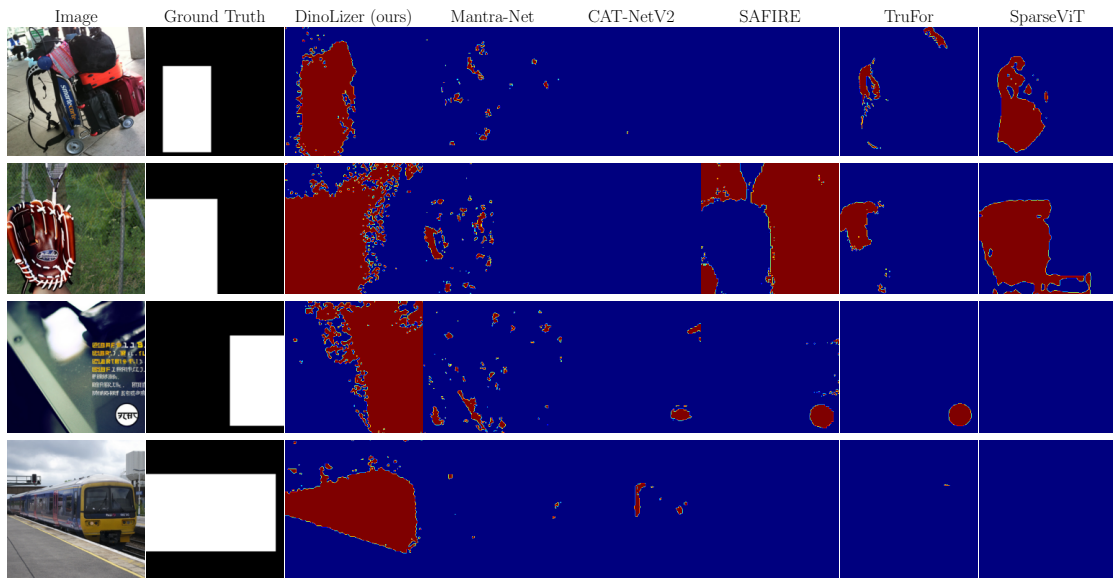


Figure 16: Visual comparison of forgery localization results on the B-Free dataset.